Current Biology 16, 833–844, May 9, 2006 ©2006 Elsevier Ltd All rights reserved DOI 10.1016/j.cub.2006.03.038

Article

Integrin $\alpha_5\beta_1$ and Fibronectin Regulate Polarized Cell Protrusions Required for *Xenopus* Convergence and Extension

Lance A. Davidson,[1,2,3,*] Mungo Marsden,[1,4] Raymond Keller,[2] and Douglas W. DeSimone[1]
[1] Department of Cell Biology
University of Virginia Health System
Charlottesville, Virginia 22904
[2] Department of Biology
University of Virginia
Charlottesville, Virginia 22904

Summary

Background: Integrin recognition of fibronectin is required for normal gastrulation including the mediolateral cell intercalation behaviors that drive convergent extension and the elongation of the frog dorsal axis; however, the cellular and molecular mechanisms involved are unclear.
Results: We report that depletion of fibronectin with antisense morpholinos blocks both convergent extension and mediolateral protrusive behaviors in explant preparations. Both chronic depletion of fibronectin and acute disruptions of integrin $\alpha_5\beta_1$ binding to fibronectin increases the frequency and randomizes the orientation of polarized cellular protrusions, suggesting that integrin-fibronectin interactions normally repress frequent random protrusions in favor of fewer mediolaterally oriented ones. In the absence of integrin $\alpha_5\beta_1$ binding to fibronectin, convergence movements still occur but result in convergent thickening instead of convergent extension.
Conclusions: These findings support a role for integrin signaling in regulating the protrusive activity that drives axial extension. We hypothesize that the planar spatial arrangement of the fibrillar fibronectin matrix, which delineates tissue compartments within the embryo, is critical for promoting productive oriented protrusions in intercalating cells.

Introduction

The extracellular matrix (ECM) plays a major role in the development of metazoans. Many ECM molecules function as adhesive ligands and can signal through transmembrane receptors such as integrins and syndecans [1] or can act as scaffolds that bind and restrict the diffusion of growth factors involved in attracting, repelling, or guiding cells during their migrations [2, 3]. One component of the ECM, fibronectin (FN), and the integrin receptors that bind it play central roles in morphogenesis [4, 5]. In FN-deficient mice, gastrulation appears to proceed normally in anterior tissues but fails posteriorly [6]. Similarly, the phenotypes of embryos lacking integrin α_5, the predominant FN receptor, are generally less severe than the FN null phenotype [7, 8]. However, in both cases axial extension is significantly reduced, indicating that more subtle defects in gastrulation movements may be responsible. Additional evidence supporting a critical role for integrin and FN in gastrulation comes from work on salamanders [9–12] and more recently the frog *Xenopus laevis* [5, 13–16]. Thus, integrin-FN interactions participate in a variety of processes that precede the cell movements responsible for convergence and extension and tissue migration. What has not been addressed by these studies is the relationship between integrin-FN engagement and the regulation of mediolateral cell intercalation behaviors that drive convergence and extension.

The narrowing and coordinate lengthening, or convergent extension, of embryonic tissues by cell intercalation is a recurring theme in chordate and invertebrate development [17] with many pathways involved in its regulation. Convergent extension of the dorsal mesoderm in *Xenopus* is driven largely by mediolateral intercalation of postinvolution mesodermal cells [18] as cells extend polarized tractive protrusions at their medial and lateral ends [19]. The cell movements and molecular pathways that regulate convergence and extension have been the subject of intense research in recent years (for reviews, see [20–25]). Recently, components of the extracellular matrix and their cell-surface receptors have been implicated in this behavior [13, 16, 26].

A key question is whether the requirement for cell-FN interactions at gastrulation reflects an adhesive/mechanical role that promotes cell traction and intercalation, or whether the matrix provides instructional information that permits the establishment of polarized protrusive behaviors. In this study, we provide evidence that a FN matrix and signaling through integrin $\alpha_5\beta_1$ are required for productive, oriented protrusions that drive mediolateral cell intercalation and convergent extension.

Results

Fibronectin Protein "Knockdown" Retards Gastrulation and Blocks Convergence and Extension

We repressed FN protein synthesis with antisense morpholino oligonucleotides directed against the two FN genes expressed in the early embryo [27]. FN levels were reduced by 85% to 95% (n = 3; 10 embryos per sample per experiment) relative to control embryos when coinjected with 6.0 to 7.5 μMoles of each antisense morpholino (FNMO; Figure 1A). Patterning of axial mesoderm was unaffected, whereas convergence of the dorsal axial mesoderm was reduced by 20% as shown by a wider region of chordin expression (arrows in Figure 1B), which marks the prospective notochord.

*Correspondence: ldavidson@engr.pitt.edu
[3] Present address: Department of Bioengineering, University of Pittsburgh, Pittsburgh, Pennsylvania 15260.
[4] Present address: Department of Biology, University of Waterloo, Waterloo, Ontario N2L 3G1, Canada.

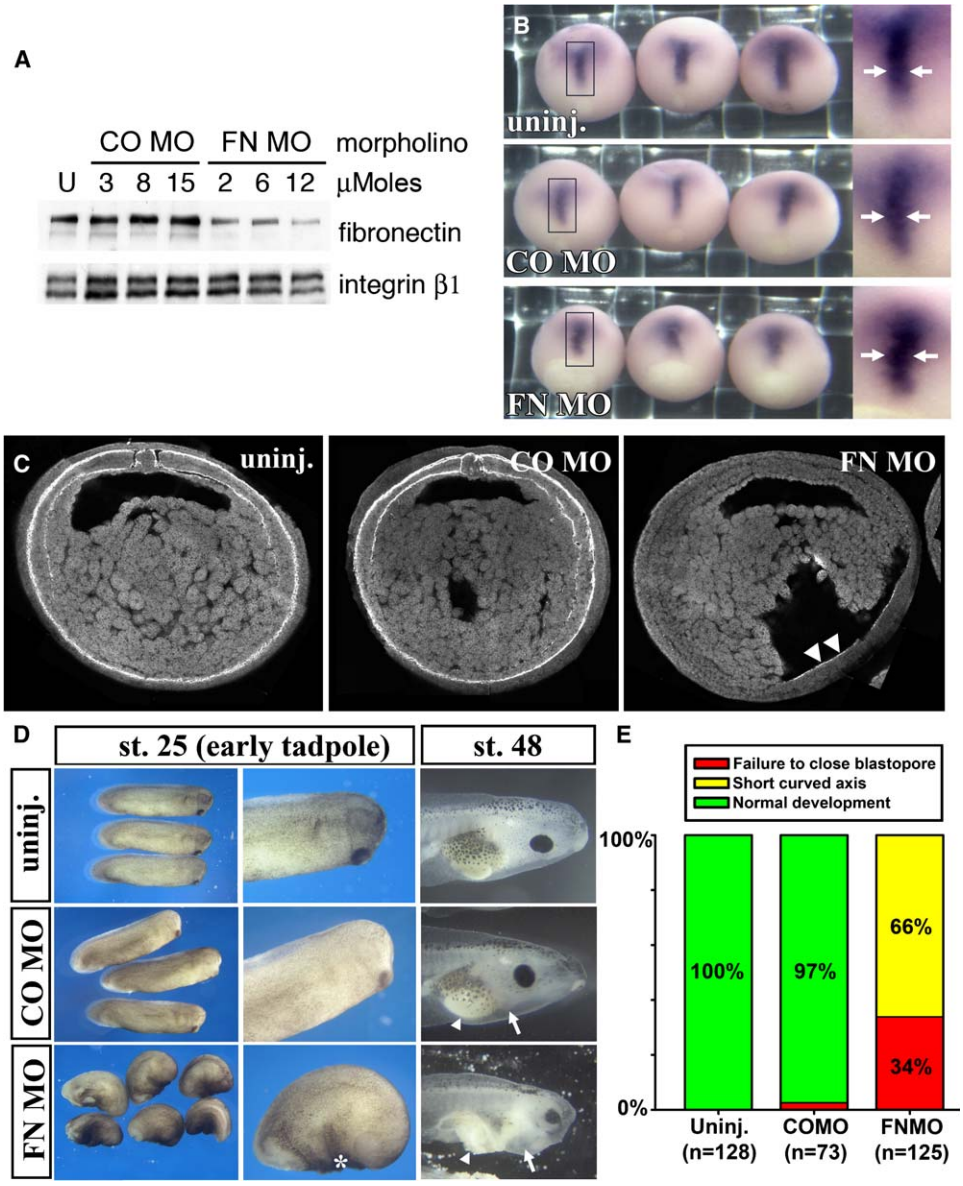

Figure 1. FN Antisense Morpholino "Knocks down" FN Protein Synthesis, Reduces Fibril Formation, and Reduces Dorsal Axis Extension

(A) Western blot analysis of morpholino (MO)-injected embryos harvested at stage 10.5 and processed for detection with the anti-FN mAb 4H2 and the anti-integrin β_1 PcAb 363. The two FN bands correspond to two major alternatively spliced FN subunits expressed during development. The control MO has no affect on the levels of expression of either FN or integrin β_1 at up to 15 μMoles MO injected per embryo. A dose-dependent reduction in FN protein expression is noted in the presence of the combined (50:50) FNMOs. Levels of integrin β_1 protein expression are unaffected by the FN antisense MO.

(B) Expression of chordin, a marker of dorsal axial tissues, shows that embryos injected with 15 μMoles FNMO have wide dorsal axial tissues. (Arrows mark the width of the chordin expression.)

(C) Transverse confocal sections of embryos stained for FN fibrils show a typical pattern in both control morpholino and uninjected control embryos while fibril formation is almost completely abolished (see arrowheads for an example of faint labeling of blastocoel roof ectoderm in FNMO-injected embryos).

(D) FNMO-injected embryos show defects in both dorsal and ventral elongation by early tadpole stages and severe anterior mesoderm defects by later tadpole stages. At early tadpole stages, the dorsal axial extension is moderately reduced while ventral extension is severely reduced (asterisk). Late-stage FNMO-injected tadpoles show defects in ventral mesoderm morphogenesis, ectodermal lesions, and failure of heart (arrow) and gut (arrowheads) formation.

(E) Pooled data from three batches of embryos were observed over several days and their progress was assessed. None of the embryos injected with 15 μMoles FNMO develop beating hearts.

FNMO-injected embryos exhibit a near complete absence of FN fibrils (some fibrils are still evident on the walls of the blastocoel; Figure 1C, arrowheads), and when cultured to later stages (Figure 1D), embryos exhibit similar phenotypes (Figure 1E) to those observed after blastocoelic injection of anti-FN or anti-integrin $\alpha_5\beta_1$ function-blocking antibodies or expression of integrin β_1 dominant-negative constructs [13, 14, 28–30].

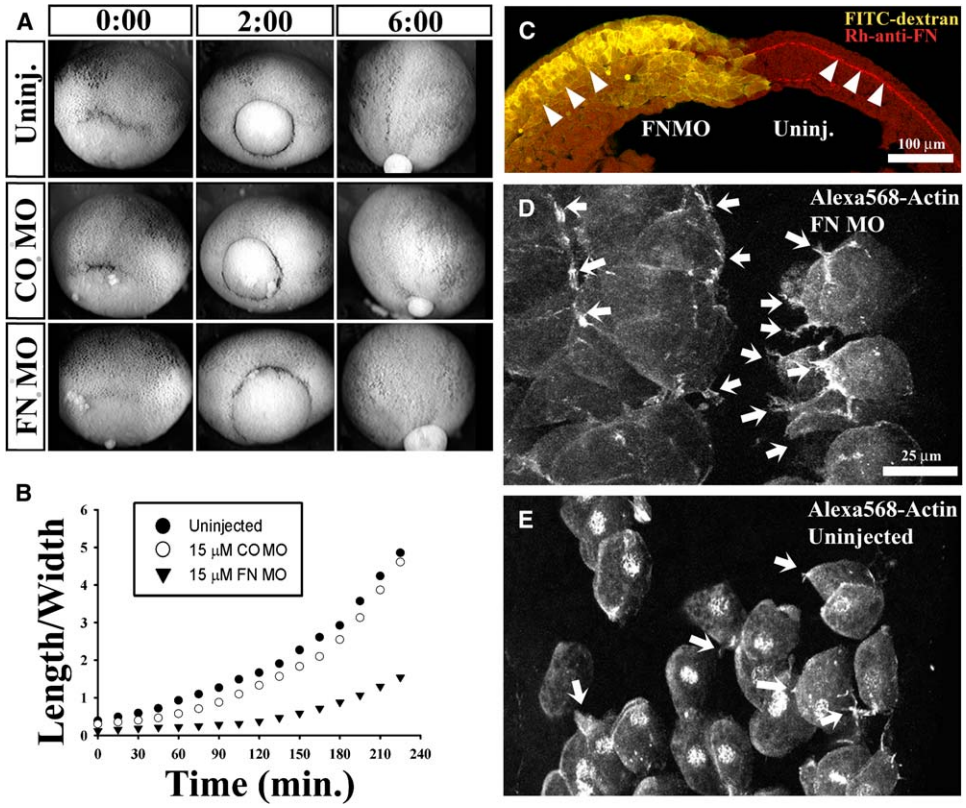

Figure 2. FN Knockdown Retards Blastopore Closure, Slows Convergence and Extension, and Produces Tissue Thickening and an Excess of Actin-Rich Cellular Extensions in Whole Embryos

(A) Frames from a representative time-lapse sequence show that blastopore closure is delayed in 15 μMoles FNMO-injected embryos until sibling control embryos reach equivalent midgastrula stage 13.

(B) Anterior-posterior length to the mediolateral width ratios of the noninvoluting marginal zone of control morpholino-injected embryos (open circles), uninjected embryos (filled circles), or FNMO-injected embryos (filled triangles) show that FNMO-injected embryos lag 2 hr behind control embryos.

(C) Transverse confocal section through the dorsal axis of an embryo injected contralaterally with FNMO along with a FITC-dextran lineage tracer shows the absence of fibrils is accompanied by tissue thickening on the injected side.

(D and E) A maximal projection of a 30 μm thick sagittal confocal stack of a region just animal of the blastopore lip at stage 11.5 show that actin-rich cellular extensions are abundant in FNMO-injected embryos (D) but far less common within uninjected embryos (maximal projection of a 60 μm sagittal confocal stack; [E]).

FNMO-injected embryos cultured to tadpole stages eventually recover fibrils (data not shown) and will extend, but they continue to lack anterior mesodermal tissues such as gut and heart (Figure 1D).

Frames from time-lapse sequences show that FNMO-injected embryos are slow to close their blastopores relative to control embryos (Figure 2A, 2:00 hr), a sign of defective convergence and extension [31, 32], but most (Figure 1E) continue to involute and eventually complete blastopore closure by 6 hr (Figure 2A). Convergence and extension of the noninvoluting marginal zone (NIMZ) is delayed for approximately 2 hr in FNMO-injected embryos based on the calculated length to width ratio (anteroposterior length/mediolateral width) of the NIMZ from 2 to 6 hr after the start of gastrulation (Figure 2B).

We then injected embryos with 7.5 μMoles FNMO and a FITC-dextran lineage tracer into a single blastomere at the 2-cell stage and cultured the embryos to midgastrula stages (stage 11.5) before fixing and staining FN fibrils (Figure 2C). Transverse confocal sections reveal that such embryos fail to assemble FN along the mesoderm-neural ectoderm interface [16] on the injected side (arrowheads; Figure 2C), which always remains thicker than the control sides. To resolve whether cells in FNMO-injected embryos had defective cellular extensions such as lamellipodia or filopodia, we observed actin-rich protrusions within scattered cells in an otherwise unlabeled embryo [16]. Single blastomeres were injected with Alexa-568 actin at the 16- or 32-cell stage. Embryos were cultured and fixed at mid-gastrula (stage 11.5), and high-resolution confocal sagittal sections were collected from just within the region of the blastopore lip. Cells within FNMO-injected embryos have an abundance of actin-rich protrusions (Figure 2D). In contrast, uninjected cells located within the same comparable region extend far fewer actin-rich protrusions from their surface (Figure 2E).

Keller sandwich explants expressing FNMO converge but extend poorly after 6 hr (Figure 3A; in Figure 3B compare the animal ectoderm half of the explant that does not converge [arrows] to the mesodermal half [arrowheads]). FN fibrils are dramatically reduced in these sandwich explants compared to explants prepared

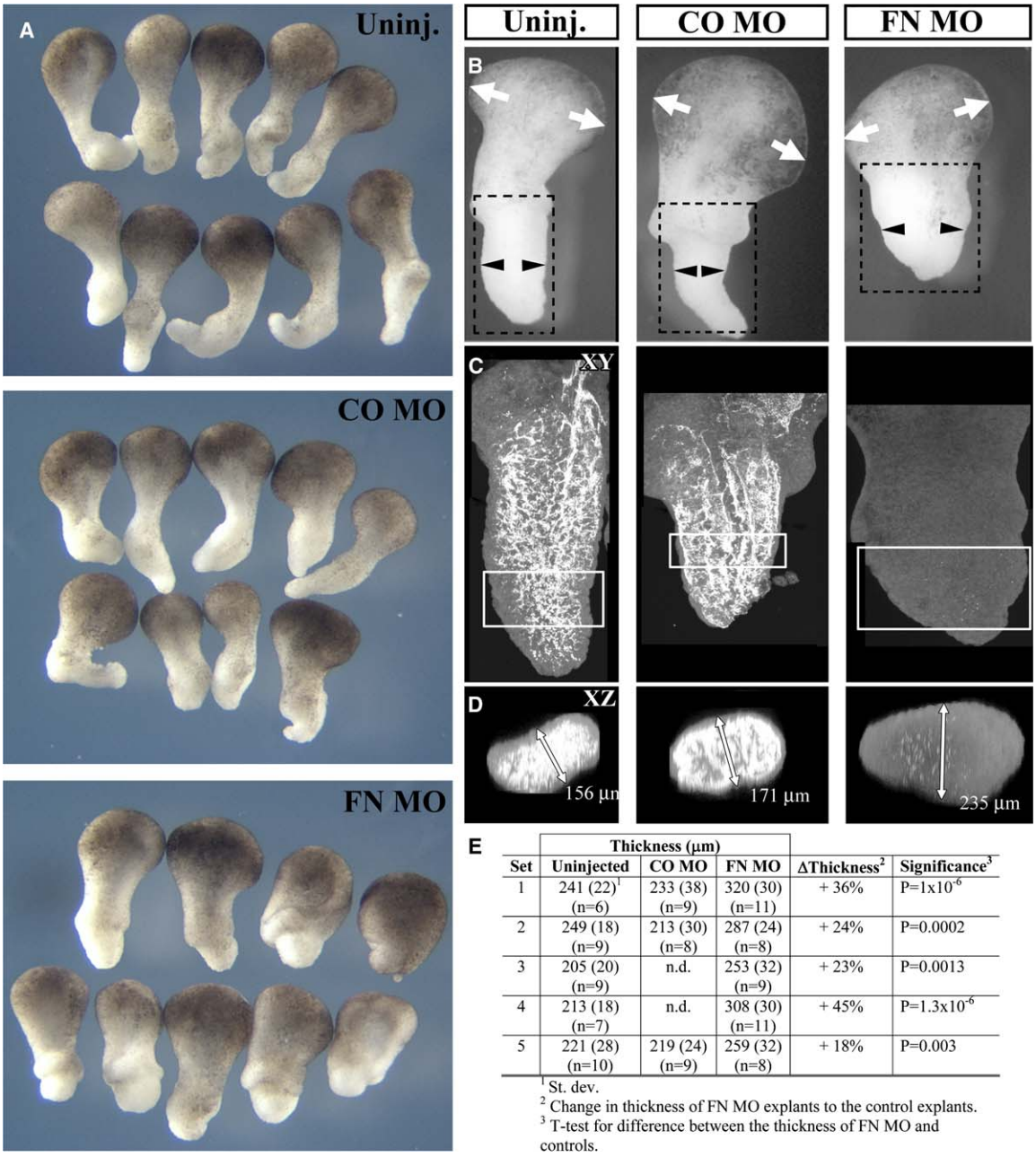

E

Set	Thickness (µm) Uninjected	CO MO	FN MO	ΔThickness[2]	Significance[3]
1	241 (22)[1] (n=6)	233 (38) (n=9)	320 (30) (n=11)	+ 36%	$P=1x10^{-6}$
2	249 (18) (n=9)	213 (30) (n=8)	287 (24) (n=8)	+ 24%	P=0.0002
3	205 (20) (n=9)	n.d.	253 (32) (n=9)	+ 23%	P=0.0013
4	213 (18) (n=7)	n.d.	308 (30) (n=11)	+ 45%	$P=1.3x10^{-6}$
5	221 (28) (n=10)	219 (24) (n=9)	259 (32) (n=8)	+ 18%	P=0.003

[1] St. dev.
[2] Change in thickness of FN MO explants to the control explants.
[3] T-test for difference between the thickness of FN MO and controls.

Figure 3. FN Knockdown Retards Convergence and Extension in Sandwich Explants

(A) Representative 6-hr-old Keller sandwich explants from 15 µMoles FNMO-injected embryos show convergent thickening but little extension, while uninjected sandwiches and control morpholino-expressing explants (COMO) converge and extend.

(B) Individual explants showing convergence of the mesoderm with respect to the ectoderm (arrowheads versus arrows) were stained for fibronectin fibrils.

(C) Montages of en face maximal projections of confocal z-series of FN fibrils from the same explants shown in ([B]; dashed boxes) show that fibrils do not assemble in FNMO-expressing explants while fibrils assemble in control explants.

(D) XZ-projections analogous to transverse projections of confocal z-series (shown by white boxes in [C]) show that fibrils assemble within control explants but not within the thicker sandwich explants made from FNMO-injected embryos. Arrow-ended lines indicate thickness of explant.

(E) Measurements of explant thickness from five batches of sandwich explants demonstrate FNMO-expressing explants are significantly thicker than sibling control or COMO-injected explants.

from either uninjected or control morpholino-injected (COMO) embryos (Figure 3C). Furthermore, transverse views reveal that FNMO-injected explants remain thick (Figure 3D). The significant convergence movements that occur in these explants result in thickening of the tissue rather than axial extension (Figure 3E).

Exogenous Fibronectin Substrate Rescues Cell Elongation and Polarized Cell Behaviors in FNMO Explants Lacking Fibronectin Fibrils

To confirm that the phenotypes observed by means of the antisense morpholinos were a direct consequence of reduced FN expression, we cultured marginal zone

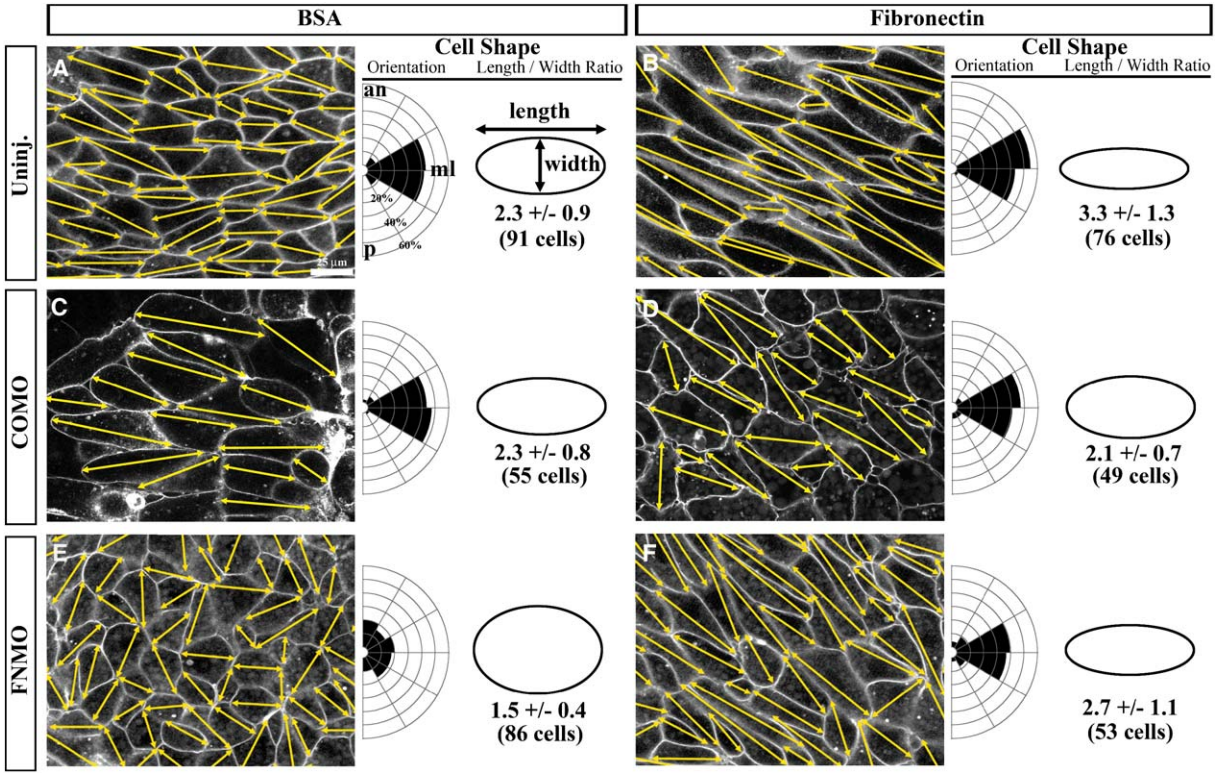

Figure 4. Mediolaterally Oriented Cell Elongation Can Be Rescued by Planar FN

(A–D) Mesoderm cells within confocal sections collected at 6 μm depth from 6-hr-old control uninjected or COMO-injected explants expressing a membrane localizing GFP exhibit characteristic bipolar shape with length to width ratios (LWR) greater than 2.0 when cultured either on BSA (A and C) or on FN (B and D). Cells that exhibit high LWRs align strongly to the mediolateral axis.

(E) Explants from embryos injected with 15 μMoles of FNMO do not develop bipolar cell shapes, exhibit a low LWR when cultured on BSA, and do not align to the mediolateral axis.

(F) However, when presented with a FN-coated glass coverslip cells intercalate, become elongated with LWRs similar to control explants on FN, and align strongly to the mediolateral axis.

Rose diagrams in each panel show the angular distribution of cells' long axes with respect to the mediolateral axis. The ellipse in each panel represents the average cellular LWR. The error is the standard deviation for the number of cells measured. Yellow arrows indicate orientation of the long axis in each individual cell. In each case, analyzed cells come from a single representative explant.

explants on FN-coated and nonadhesive substrates. Mesoderm cells within uninjected or COMO-injected explants elongate along the mediolateral axis (ML) after 6 hr either on BSA (Figures 4A and 4C; chi-square test against randomness, $p = 6.3 \times 10^{-6}$ or $p = 2.2 \times 10^{-16}$, respectively) or FN-coated substrate (Figures 4B and 4D; $p = 8.2 \times 10^{-15}$ or $p = 6.2 \times 10^{-13}$). In contrast, mesoderm cells in explants injected with FN morpholinos cultured on BSA neither elongate nor orient (Figure 4E; chi-square test against randomness, $p = 0.59$). Culturing FNMO-injected explants on FN restored cell elongation with cells strongly aligned with ML (Figure 4F; $p = 1.3 \times 10^{-12}$). Thus, the FN morpholino prevents assembly of FN fibrils but does not alter ability of the explant to respond to an exogenously supplied FN substrate.

Bipolar Protrusive Activity on Fibronectin

To observe mediolateral intercalation behavior (MIB), we used explants cultured on a FN substrate (see [33]), a preparation that allows expression of the characteristic bipolar mediolaterally oriented protrusive activity and cell elongation observed originally in the "shaved explant" ([19]; see Supplemental Data available with this article online). We simultaneously imaged cell-substrate level protrusive activity (Figure 5A) and deeper (5 μm) cell-cell protrusive behavior (Figure 5B) with high-resolution confocal time-lapse microscopy and a plasma membrane-localized GFP (gap43-GFP; [34]) to delineate cell boundaries. "Dual-level" time-lapse sequences were assembled (Figure 5C; see time-lapse sequence, Movie S2) and used to track lamellipodia on the substrate with respect to the center of mass at both levels (Figure 5D). In a typical explant, cells send out 12 lamellipodia per hour (Figure 5E; n = 166), and each lamellipodia lasts on average 5.5 min (Figure 5F; n = 166). When the orientations of all lamellipodia seen at the level of the substrate (i.e., 0 μm depth) are combined, a clear mediolateral bias emerges (Figure 5G; 166 lamellipodia in 30 cells over 25 min; chi-square test of randomness, $p = 4.7 \times 10^{-10}$). Large protrusions at the 5 μm depth also exhibit a mediolateral bias (Figure 5H) as cells elongate. Interestingly, long-lived lamellipodia, persisting longer than 4 min (black, Figure 5I), are strongly oriented, with 77% of them being directed into mediolateral quadrants, whereas only 59% of those lasting less than 4 min (gray, Figure 5I) are directed mediolaterally (chi-square test against randomness, $p = 2.7 \times 10^{-7}$ and 0.016, respectively).

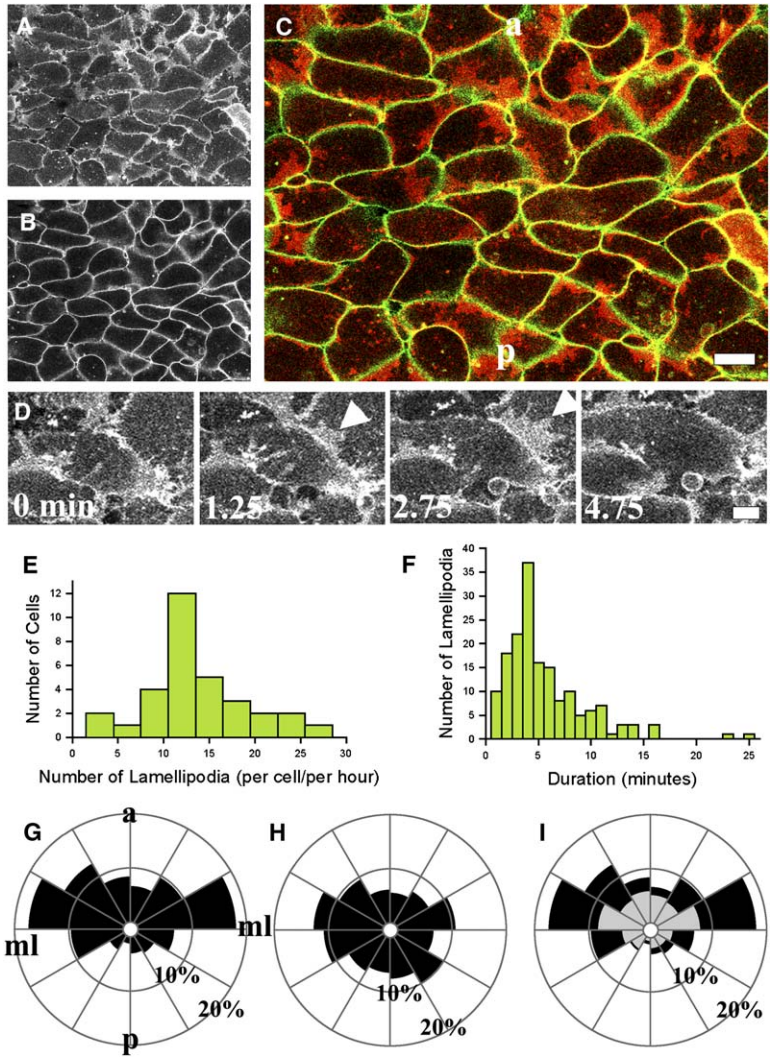

Figure 5. Two-Plane Confocal Time-Lapse Sequence of MZ Explants Cultured on FN Show Cell Behaviors during Mediolateral Cell Intercalation

(A–C) Optical sections from the plane of the FN-coated coverslip (A) and from 5 μm deeper in the explant (B) were collected at 15 s intervals and combined into a two-color time-lapse sequence (C) where cell identities and cell shapes were correlated with protrusions. Our dual-level imaging technique is required for the analysis of cellular behaviors, for instance confirming the identity of cellular protrusions in the neighborhood of triple-cell junctions, and is critical to our interpretation of cellular protrusions over the time course of an acute experiment, for instance in determining the onset of explant shear, which can produce shingled cells that are easily mistaken for monopolar protrusive cells.

(D) Single lamellipodia can be identified (arrowhead), their duration measured, and their orientation determined with regard to both the cell and the mediolateral axis of the explant.

(E) A frequency distribution of 166 lamellipodia extended on the FN-coated coverslip is shown for 32 cells in the reference explant shown in (A).

(F) The life-time distribution, from initiation to retraction, of these lamellipodia.

(G and H) Rose diagrams demonstrate that most lamellipodia at the surface (G) are mediolaterally oriented, as are deep cell extensions shown in (B) at the 5 μm level (H).

(I) Long-lived lamellipodia (black) are found at the mediolateral ends of cells whereas short-lived lamellipodia (gray) are more randomly oriented. Scale bar in (C) is 25 μm and in (D) is 10 μm (a, anterior; p, posterior; ml, mediolateral). This time-lapse sequence can be viewed in Movie S2.

Establishment and Maintenance of Bipolar Protrusive Activity Requires Continued Integrin/FN Interactions

Cell behaviors change considerably when FNMO-injected explants are presented with a planar FN substrate (n = 4; Figures 6A and 6B; compare difference time-lapse sequences; see time-lapse sequences, Movies S3 and S4). Cell protrusions within FNMO explants on BSA are not ML oriented (see Figure S3 for angular distributions; 29.7% of protrusions were aligned within 30° of ML and 26.3% were aligned within 30° of the anteroposterior axis, AP) while cells in FNMO explants cultured on FN have a bipolar distribution of protrusions (68% directed ML and 11.5% directed AP). The appearance of the bipolar distribution of protrusions in FNMO-injected explants cultured on FN was accompanied by a lower frequency of lamellipodia than seen in FNMO-injected explants cultured on BSA (Figure 6C). In contrast to the lamellipodial frequency, the persistence of lamellipodia was unchanged (see Figure S3C for lamellipodia persistence).

Rapid and dramatic changes in protrusive activity are observed shortly after addition of the integrin $\alpha_5\beta_1$ function-blocking monoclonal antibody (mAb P8D4 [15]; n = 5; Figures 6D and 6E; see time-lapse sequence and difference sequence, Movies S5 and S6). The typical bipolar distribution of protrusions is lost after addition of P8D4 (before P8D4, 56.1% of lamellipodia align within 30° of ML and 25.4% align with the anteroposterior axis; after P8D4, 23.9% align with ML and 45.1% with AP), and the rate of protrusions increases sharply ($p = 9.1 \times 10^{-5}$; Figure 6F). In contrast, duration of lamellipodia is unchanged (see Figure S3F). Application of a control antibody (mAb 4H2) has no effect (data not shown). Thus, both the establishment and maintenance of mediolaterally directed protrusive activity requires integrin $\alpha_5\beta_1$ recognition of FN.

FN/Integrin Interactions Suppress Random Protrusions in Favor of Polarized Protrusions

To test whether the $\alpha_5\beta_1$-blocking antibody P8D4 may function as a ligand mimetic superactivating $\alpha_5\beta_1$ and induce rapid protrusive activity, explants were cultured directly on substrates coated with mAb P8D4. The explants adhered but did not undergo mesendodermal or ectodermal migration (data not shown), both of which are normally regulated by cell recognition of the central cell binding domain (CCBD) of FN through integrin $\alpha_5\beta_1$

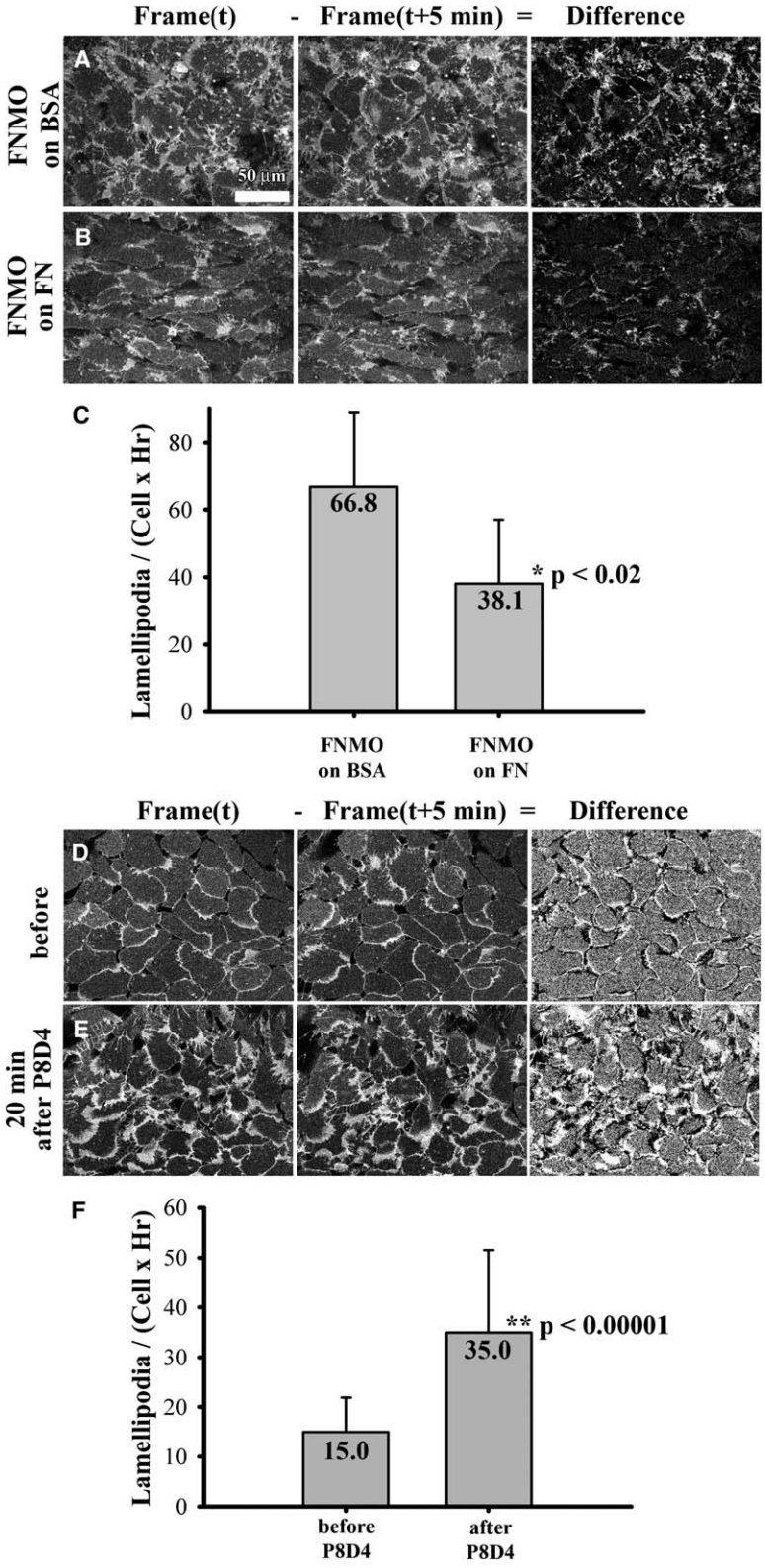

Figure 6. Mediolateral Cell Intercalation Behaviors in FN Knockdown Explants Are Rescued when Cells Provided with a Planar FN-Substrate while Blocking Integrin $\alpha_5\beta_1$ Stimulates Cell Protrusive Activity

(A and B) Two frames from representative confocal time-lapse sequences of 15 μMoles FNMO-injected explants expressing GAP43-GFP and their calculated "difference" images were calculated for explants cultured on BSA ([A]; see Movie S3) and on fibronectin ([B]; see Movie S4). A "difference time-lapse" sequence shows regions of cell protrusion and retraction as solid white and black regions, respectively, while regions where little change occurs are typified by gray.

(C) Culture of FNMO-injected explants on FN significantly represses the rate of protrusions.

(D–F) Two frames from a representative confocal time-lapse sequence and their calculated "difference" image before (D) and after ([E]; see Movies S5 and S6 for difference time-lapse sequence) addition of 0.1 μg/ml of the integrin $\alpha_5\beta_1$ function-blocking antibody P8D4 to the explant show that protrusive behaviors are stimulated and the rate of protrusive activity increases (F).

The time-lapse sequences, in two-level form, and the difference time-lapse sequence can be viewed in Supplemental Data.

[29]. Thus, it is unlikely that mAb P8D4 acts as a simple mimetic ligand for $\alpha_5\beta_1$ (i.e., the CCBD of FN and mAb P8D4 are not functionally equivalent in these assays). Alternatively, mediolaterally oriented cell protrusive activity in the presence of intact FN-integrin interactions may reflect a repression of random protrusions, which is "relieved" when FN levels are reduced with FNMO or when $\alpha_5\beta_1$ binding to FN is blocked by mAb P8D4 (Figure 6). We tested this hypothesis by "activating" integrins with Mn^{2+} [35–37] in order to assess whether protrusive activity decreased. Addition of $MnCl_2$ to 1 mM final concentration produces a more quiescent

explant with fewer lamellipodia (n = 4; compare difference frames of Figures 7A and 7B). In a representative time-lapse sequence, protrusive rates drop sharply (Figure 7C; Student's t test, p = 0.02). However, in contrast to the effect of the integrin function-blocking antibody, the bipolar distribution of protrusions (61.8% are directed within 30° of the ML axis and 9.1% are directed along the AP axis) is not lost in the presence of Mn^{2+} (36.9% directed ML and 5.2% directed AP; see Figure S3G).

Exogenous Integrin Activation Represses Protrusive Activity even when $\alpha_5\beta_1$ Integrin Function Is Blocked

We next investigated whether Mn^{2+} could repress the high rate of protrusions under conditions where normal integrin engagement of FN is blocked (n = 4; Figures 6D–6F). We applied 1 mM $MnCl_2$ to explants that had already incubated for over 1 hr in 0.1 mg/ml P8D4 and observed protrusive behaviors (Figures 7D and 7E). We observed that the high rates of protrusions in explants cultured in P8D4 drop 47% after addition of Mn^{2+} (p = 0.02; Figure 7F). In this case, addition of Mn^{2+} also increases the persistence of lamellipodia by 62% ($p = 2 \times 10^{-8}$; see Figure S3L). However, the rescue of protrusive behaviors is not complete since a bipolar distribution of protrusions is not restored after addition of Mn^{2+} (Figure S3J). Before addition of Mn^{2+}, 41.0% of protrusions align within 30° of the ML axis and 30.2% align with the AP axis. After addition of Mn^{2+}, 36.1% of lamellipodia align with ML and 20.6% align with AP. Thus, activation of integrin with Mn^{2+} is sufficient to repress high rates of protrusive activity in the absence of integrin binding to endogenous ligand.

Discussion

In our experiments, both chronic deficits in FN synthesis (i.e., by means of antisense morpholinos) and the acute affects of blocking integrin $\alpha_5\beta_1$ binding to FN (i.e., by mean of a monoclonal antibody) demonstrate that mediolateral cell protrusive activity, the principal polarized cell behavior that drives axis extension, is dependent upon recognition of FN matrix by integrin (Figure 8A). The FN-specific antisense morpholinos used in this study were highly effective at reducing FN protein synthesis from both maternal and zygotic mRNAs, and the resultant phenotypes observed mimicked those obtained by blastocoelic injection of anti-FN function-blocking mAbs [14] or expression of an integrin dominant-negative construct [13]. In addition, cell behaviors could be rescued fully by providing FN protein to explants lacking endogenous FN. Attempts to rescue intact FNMO-injected embryos by injecting mammalian plasma FN into the blastocoel was partially successful (data not shown), but the degree of recovery varied widely from experiment to experiment. The kinetics of FN assembly at cell surfaces is complex, and our inability to reliably obtain a rescue in whole embryos may reflect the timing of assembly in vivo, nonoptimal FN concentrations, and/or inefficient incorporation of heterologous FN into fibrils.

Organized ECM Is Required for Vertebrate Gastrulation

The assembly of a fibrillar matrix is required for gastrulation and may serve as a checkpoint for the progression of subsequent morphogenetic movements. Gastrulation movements are disrupted in embryos lacking FN (this study; [14]) and may become misdirected when fibrils are deposited at inappropriate locations [26] or times. How malformed and/or absent FN fibrils affect cell movements is unclear, but alterations in the physical-mechanical properties of the ECM and adjacent tissues may be responsible. For example, reductions in fibril density could alter the stiffness of the axial mesoderm and reduce the normal rigidity of this tissue, which is critical for convergence and extension [38]. To operate as a cell signaling checkpoint, recognition of FN fibrils may trigger postinvolution behaviors such as mediolateral cell intercalation. Failure to assemble fibrils may lead to dysregulation of the normal temporal and spatial patterns of adhesive behaviors that are required for gastrulation movements by altering integrin activation [28] or cadherin affinity [13, 39, 40].

ECM Maintains Polarized Protrusive Activity

Mediolateral cell intercalation requires reiterated cycles of polarized protrusions that may be linked to the regulation of integrin activation state. Dramatic differences in mesodermal cell behaviors are noted following the addition of the integrin $\alpha_5\beta_1$ function-blocking antibody or $MnCl_2$, which resulted in a switch to either a higher or lower rate of protrusive activity, respectively. Mn^{2+} is thought to act by "locking" integrins into a conformation that approximates the ligand bound state [41] while the P8D4 antibody blocks integrin binding to ligand. Because both of these acute-acting agents are exogenously applied, it is unlikely that any spatially localized patterns of integrin activation are maintained in their presence. However, mediolateral intercalation may not be regulated by designated subcellular domains of integrin activation but instead by tight control of regions where integrins are maintained in an "inactivated" state.

Loss of polarized protrusive activity is observed in explants derived from FNMO-injected embryos and in wild-type explants cultured in the presence of the anti-$\alpha_5\beta_1$ blocking antibody (Figure 6). One significant difference noted between these preparations is the elongate morphology of cells, which is absent in the FNMO explants but retained in explants treated with the antibody. Interestingly, cells in antibody-treated explants maintain elongate morphology even while progressively losing the mediolateral orientation of their long axes (see Figures S3D and S4). In the case of the morpholino experiment, it is likely that the cells in these explants were unable to establish an elongate shape in the absence of FN. In contrast, cells in the wild-type explants are already beginning to elongate prior to the addition of blocking antibody and do not significantly change shape after the addition of antibody (see Supplemental Results and Figure S4). Thus, once established, elongate cell shape is maintained even in the absence of continued recognition of FN by $\alpha_5\beta_1$. This highlights the importance of "acute" approaches to understanding cell behaviors as a complement to "chronic" loss-of-function strategies (e.g., targeted knockout, knockdown, or mutational analyses).

ECM Coordinates Cell Behaviors at the Tissue Level

Integrin function-blocking experiments suggest two different ways in which the fibrillar FN ECM (Figure 8B)

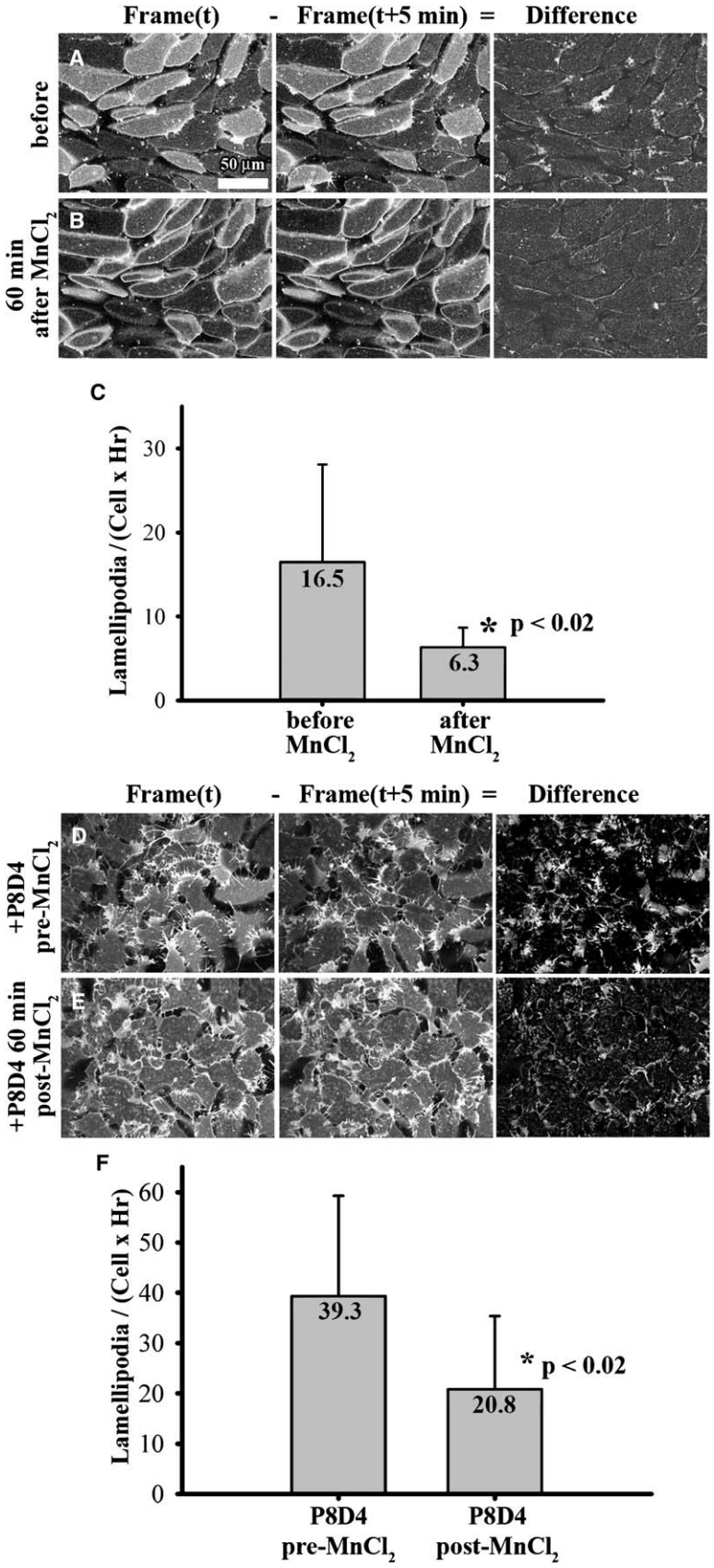

Figure 7. Integrin "Superactivation" Represses Protrusive Activity

(A and B) Two frames from a representative confocal time-lapse and their calculated difference image before (A) and after (B) superactivation of integrins after addition of 1 mM $MnCl_2$ demonstrate repression of protrusive activity.

(C) Rates of protrusive activity drop 3-fold after addition on $MnCl_2$.

(D and E) Two frames from a representative confocal time-lapse sequence and their calculated difference image before (D) and after (E) superactivation of integrin after addition of 1 mM $MnCl_2$ demonstrate repression of protrusive activity in explants already incubated for 1 hr in 0.1 μg/ml of the integrin $\alpha_5\beta_1$ function-blocking antibody P8D4.

(F) Addition of $MnCl_2$ results in a 2-fold reduction in rates of protrusions.

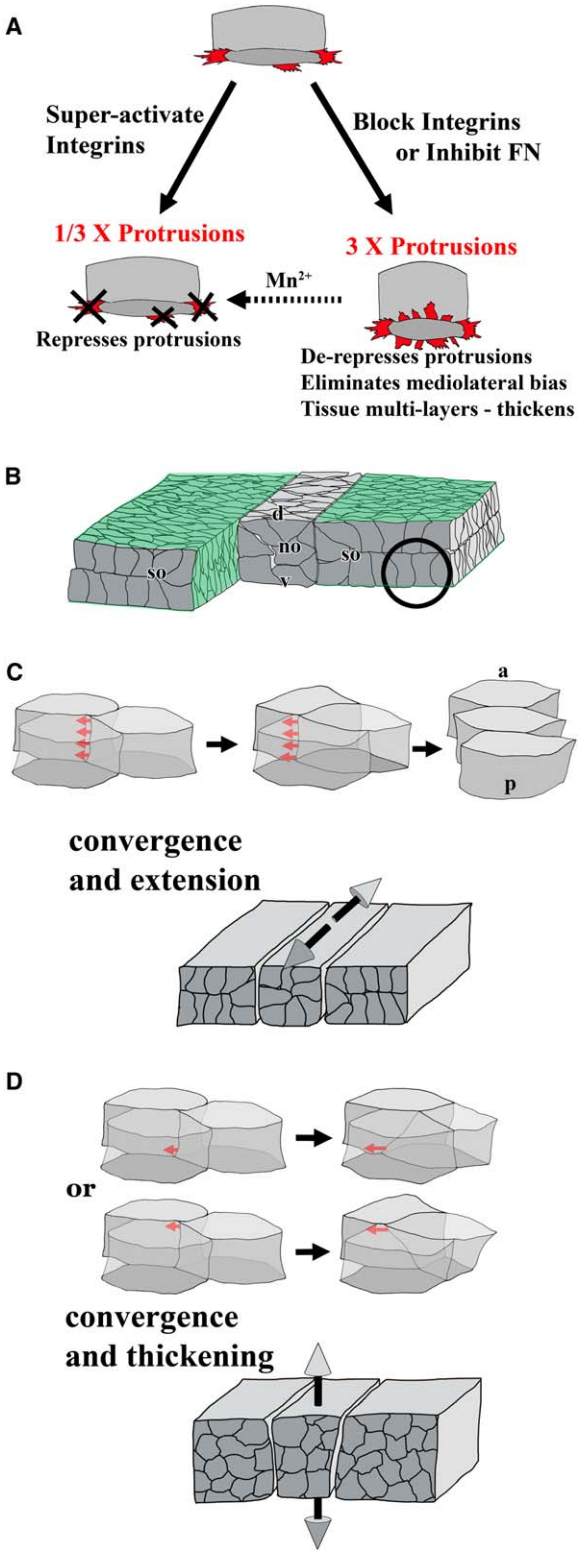

Figure 8. ECM Regulation of Convergence and Extension

(A) Control of protrusive rates and orientation by FN/integrin interactions. Superactivation of integrins with Mn^{2+} results in reduced protrusive rates whereas removal of FN fibrils or inhibition of $\alpha_5\beta_1$ enhances the frequency of protrusions and results in loss of mediolateral orientation.

(B) Effective convergence and extension requires maintenance of a two-cell layered mesoderm. Closer inspection of mediolateral cell intercalation (within circle) reveals an underlying cellular mechanism.

(C) Tractive protrusions (red arrows), balanced along mediolateral contacts with neighboring cells, directs cell intercalation and separates neighboring cells along the anterior-posterior axis (a, anterior; p, posterior). Balanced, directed intercalation maintains the two-cell layers of the mesoderm and leads to the efficient conversion of convergence into axial extension.

(D) Without a balance of forces, tractive protrusions may be directed either over the top of neighboring cells or underneath neighboring cells (single red arrows). In this case, cells converge to the midline but become multilayered. Without maintenance of two-cell layers, cell intercalation results in tissue thickening.

All views are "cut-away" transverse perspectives, centered on the notochord where the mediolateral axes run left and right and the anterior posterior axis runs toward and away (no, notochord; so, somitic mesoderm; ne, neural ectoderm; en, endoderm; d, dorsal; v, ventral).

could regulate mediolateral cell intercalation. First, fibrils may act to repress protrusions directed along the fibrillar matrix and enhance traction generated by cell-cell adhesions (Figure 8C). This regulatory mechanism would prevent cells from crawling under their neighbors, an event that produces tissue thickening rather than tissue extension (Figure 8D). Successful assembly of a fibrillar matrix could serve to maintain the tissue architecture that guides cell rearrangement into axial extension. Fibrils could encourage "restorative" radial intercalation, i.e., confining or channeling cell intercalation along exclusively planar paths rather than cell-layer "jumping" (e.g., radial "deintercalation"). An example of this role for FN fibrils can be seen during epiboly when fibrillogenesis is blocked [14]; without FN fibrils, the 2-cell layers of the ectoderm become unstable and form multiple layers. In this instance, tissue thickening results when cells fail to properly orient the spindle plane during cell division and/or when cells leave the surface of the blastocoel after radial deintercalation. Another way fibrils might regulate mediolateral cell intercalation is to repress short-duration random protrusions and encourage persistent, mediolaterally directed protrusions. This regulatory mechanism directs cell intercalation between mediolateral neighbors rather than between anterior or posterior neighboring cells. Intercalation between anterior and posterior neighbors reduces the effectiveness of directed cell intercalation in driving extension of mesoderm along the anterior-posterior axis. Both of these mechanisms operating at the scale of individual cells would regulate the progress of morphogenesis on the tissue level.

Experimental Procedures

Frogs, Explants, Antibodies, and Acute Treatments

Embryos were obtained by standard methods [42] and staged according to Nieuwkoop and Faber [43]. To label the plasma membrane of embryos, eggs were injected with 0.2 to 1 ng of capped mRNA (Epicentre, Madison, WI) encoding gap43-GFP [44]. In order to obtain scattered fluorescent labeled cells, blastomeres at the 32- to 128-cell stages were injected with approximately 2 ng/(number of blastomeres in the embryo) of rhodamine-conjugated 10 kDa dextran amine (Molecular Probes, Eugene, OR). We microsurgically isolated marginal zone explants (MZ) according to Davidson et al. [15] and cultured them in Danilchik's For Amy (DFA; [45]).

Monoclonal antibodies 4H2 and P8D4 were prepared as described previously [15, 28, 29]. For inhibition studies, mAb P8D4

and 4H2 were used at 0.1 mg/ml in DFA. All mAbs were dialyzed against DFA.

Morpholino Design and Western Blot Analysis of FN Knockdown

Sequences used in the design of antisense morpholinos were obtained from both the published *X. laevis* FN sequence ([27]; GenBank accession # M77820) and from unpublished sequence obtained from cDNA D8 (D.W.D., unpublished data). These sequences represent the two FN pseudoalleles that are each expressed in *X. laevis* embryos [27]. Antisense morpholinos were synthesized by Gene Tools, LLC (Philomath, OR) and the sequences are as follows: (XFN1.MO) 5′-CGCTCTGGAGACTATAAAAGCCAAT-3′; (XFN2.MO) 5′-CGCATTTTTCAAACGCTCTGAAGAC-3′.

The XFN1 and XFN2 morpholinos were combined (50:50, from 1 mM stock solutions) in water and injected at up to 15 μMoles total (7.5 μMoles each morpholino, <15 nl total injection volume) per fertilized egg. Water alone and the standard Gene Tools control morpholino were used in control injections. Microinjection was carried out by standard methods [46].

Five embryos per injection were harvested for analysis at stage 10.5–11 by solubilizing at 4ºC in 100 μl of ESB (100 mM NaCl, 50 mM Tris-HCl [pH 7.5], 1% NP-40, 2 mM PMSF) containing a 1:100 dilution of a protease inhibitor cocktail (Sigma #P 2714). Samples were centrifuged at 4ºC at 14,000 × g and the soluble fraction boiled in Laemmli buffer containing 10 mM dithiothreitol and subjected to SDS-PAGE with 7% acrylamide gels [47]. Proteins were transferred to nitrocellulose and processed for Western blot analysis as described previously [48], with the anti-*Xenopus* FN mAb 4H2 [29] and ECL detection (Amersham). After detection, FN blots were stripped of primary and secondary antibodies by incubation in 2% SDS, 100 mM β-mercaptoethanol, and 50 mM Tris (pH 7.0) for 30 min at 50ºC and then reprobed for β_1 integrin with the 363 PcAb [49].

Microscopy and Image Analysis

Bulk tissue movements, gross cell movement, and cell shape changes were captured as previously described [15]. Cell protrusive activity was captured with a high numerical aperture (n.a. 1.4) 60× objective in two z-level time-lapse mode with a laser scanning confocal scan head (PCM2000, Nikon, Melville, NY) mounted on an inverted compound microscope (Nikon). Frame acquisition and assembly was carried out on a computer (PC) running image acquisition software (Compix Inc., Cranberry Township, PA). All sequences, time-lapse, and z-series were archived and transferred to a computer (PC) for subsequent analysis with image processing software (Scion-Image, β 4.0.2, a port of NIH-Image and ImageJ; Wayne Rasband, NIMH; see http://rsb.info.nih.gov/nih-image/ for NIH-Image and http://rsb.info.nih.gov/ij/ for ImageJ). When determining a cell's length to width ratio (LWR), the length corresponds to the longest axis of the cell and the width corresponds to the largest distance across the cell perpendicular to the length. Since mesodermal cells progressively elongate during gastrulation [19, 50], comparisons of LWRs were valid only for explants of comparable stage. Projections of confocal stacks were carried out with ImageJ. Statistical analysis of the directional bias of cellular protrusions was carried out [51, 52] with statistics and plotting software (SigmaPlot; SPSS Inc., Chicago, IL). Analysis of protrusive activity was carried out according to [53, 54] (see Supplemental Data).

Supplemental Data

Supplemental Data include four figures and Supplemental Results and can be found with this article online at http://www.current-biology.com/cgi/content/full/16/9/833/DC1/.

Acknowledgements

We would like to thank members of the Keller and DeSimone lab for discussions and insights. We would like to thank Fred Simon and Amy Shank for their help analyzing confocal time-lapse series. We are grateful to both E. DeRobertis and J. Miller for providing GAP43-GFP plasmid. This work has been supported the National Institutes of Health (USPHS/NICHHD R01-HD44750 to L.A.D., R01-HD25594 and R01-HD036426 to R.K., and R01-HD26402 to D.W.D.). Confocal facilities were provided by the W.M. Keck Center for Cellular Imaging at the University of Virginia.

Received: October 2, 2005
Revised: March 8, 2006
Accepted: March 10, 2006
Published: May 8, 2006

References

1. Schwartz, M.A., and Ginsberg, M.H. (2002). Networks and crosstalk: integrin signalling spreads. Nat. Cell Biol. *4*, E65–E68.
2. Saharinen, J., Hyytiainen, M., Taipale, J., and Keski-Oja, J. (1999). Latent transforming growth factor-beta binding proteins (LTBPs)—structural extracellular matrix proteins for targeting TGF-beta action. Cytokine Growth Factor Rev. *10*, 99–117.
3. Yebra, M., Montgomery, A.M., Diaferia, G.R., Kaido, T., Silletti, S., Perez, B., Just, M.L., Hildbrand, S., Hurford, R., Florkiewicz, E., et al. (2003). Recognition of the neural chemoattractant Netrin-1 by integrins $\alpha_6\beta_4$ and $\alpha_3\beta_1$ regulates epithelial cell adhesion and migration. Dev. Cell *5*, 695–707.
4. Hynes, R.O. (1999). The dynamic dialogue between cells and matrices: implications of fibronectin's elasticity. Proc. Natl. Acad. Sci. USA *96*, 2588–2590.
5. Dzamba, B.D., Bolton, M.A., and DeSimone, D.W. (2002). The integrin family of cell adhesion molecules. In Cell Adhesion: Frontiers in Molecular Biology, M. Beckerle, ed. (Oxford, UK: Oxford University Press), pp. 100–154.
6. George, E.L., Georges-Labouesse, E.N., Patel-King, R.S., Rayburn, H., and Hynes, R.O. (1993). Defects in mesoderm, neural tube and vascular development in mouse embryos lacking fibronectin. Development *119*, 1079–1091.
7. Yang, J.T., Bader, B.L., Kreidberg, J.A., Ullman-Cullere, M., Trevithick, J.E., and Hynes, R.O. (1999). Overlapping and independent functions of fibronectin receptor integrins in early mesodermal development. Dev. Biol. *215*, 264–277.
8. Yang, J.T., Rayburn, H., and Hynes, R.O. (1993). Embryonic mesodermal defects in α_5 integrin-deficient mice. Development *119*, 1093–1105.
9. Darribere, T., and Schwarzbauer, J.E. (2000). Fibronectin matrix composition and organization can regulate cell migration during amphibian development. Mech. Dev. *92*, 239–250.
10. Boucaut, J.C., Johnson, K.E., Darribere, T., Shi, D.L., Riou, J.F., Bache, H.B., and Delarue, M. (1990). Fibronectin-rich fibrillar extracellular matrix controls cell migration during amphibian gastrulation. Int. J. Dev. Biol. *34*, 139–147.
11. Boucaut, J.C., Darribere, T., Li, S.D., Boulekbache, H., Yamada, K.M., and Thiery, J.P. (1985). Evidence for the role of fibronectin in amphibian gastrulation. J. Embryol. Exp. Morphol. Suppl. *89*, 211–227.
12. Boucaut, J.C., Darribere, T., Boulekbache, H., and Thiery, J.P. (1984). Prevention of gastrulation but not neurulation by antibodies to fibronectin in amphibian embryos. Nature *307*, 364–367.
13. Marsden, M., and DeSimone, D.W. (2003). Integrin-ECM interactions regulate cadherin-dependent cell adhesion and are required for convergent extension in *Xenopus*. Curr. Biol. *13*, 1182–1191.
14. Marsden, M., and DeSimone, D.W. (2001). Regulation of cell polarity, radial intercalation and epiboly in *Xenopus*: novel roles for integrin and fibronectin. Development *128*, 3635–3647.
15. Davidson, L.A., Hoffstrom, B.G., Keller, R., and DeSimone, D.W. (2002). Mesendoderm extension and mantle closure in *Xenopus laevis* gastrulation: combined roles for integrin $\alpha_5\beta_1$, fibronectin, and tissue geometry. Dev. Biol. *242*, 109–129.
16. Davidson, L.A., Keller, R., and Desimone, D.W. (2004). Assembly and remodeling of the fibrillar fibronectin extracellular matrix during gastrulation and neurulation in *Xenopus laevis*. Dev. Dyn. *231*, 888–895.
17. Keller, R. (2002). Shaping the vertebrate body plan by polarized embryonic cell movements. Science *298*, 1950–1954.
18. Keller, R., Davidson, L., Edlund, A., Elul, T., Ezin, M., Shook, D., and Skoglund, P. (2000). Mechanisms of convergence and

extension by cell intercalation. Philos. Trans. R. Soc. Lond. B Biol. Sci. *355*, 897–922.
19. Shih, J., and Keller, R. (1992). Cell motility driving mediolateral intercalation in explants of *Xenopus laevis*. Development *116*, 901–914.
20. Keller, R., and Davidson, L. (2004). Cell movements of gastrulation. In Gastrulation: From Cells to Embryos, C. Stern, ed. (Cold Spring Harbor, NY: Cold Spring Harbor Laboratory Press), pp. 291–304.
21. Montero, J.A., and Heisenberg, C.P. (2004). Gastrulation dynamics: cells move into focus. Trends Cell Biol. *14*, 620–627.
22. Solnica-Krezel, L. (2005). Conserved patterns of cell movements during vertebrate gastrulation. Curr. Biol. *15*, R213–R228.
23. Hardin, J., and Walston, T. (2004). Models of morphogenesis: the mechanisms and mechanics of cell rearrangement. Curr. Opin. Genet. Dev. *14*, 399–406.
24. Wallingford, J.B., Fraser, S.E., and Harland, R.M. (2002). Convergent extension: the molecular control of polarized cell movement during embryonic development. Dev. Cell *2*, 695–706.
25. Ninomiya, H., Elinson, R.P., and Winklbauer, R. (2004). Anteroposterior tissue polarity links mesoderm convergent extension to axial patterning. Nature *430*, 364–367.
26. Goto, T., Davidson, L., Asashima, M., and Keller, R. (2005). Planar cell polarity genes regulate polarized extracellular matrix deposition during frog gastrulation. Curr. Biol. *15*, 787–793.
27. DeSimone, D.W., Norton, P.A., and Hynes, R.O. (1992). Identification and characterization of alternatively spliced fibronectin mRNAs expressed in early *Xenopus* embryos. Dev. Biol. *149*, 357–369.
28. Ramos, J.W., Whittaker, C.A., and DeSimone, D.W. (1996). Integrin-dependent adhesive activity is spatially controlled by inductive signals at gastrulation. Development *122*, 2873–2883.
29. Ramos, J.W., and DeSimone, D.W. (1996). *Xenopus* embryonic cell adhesion to fibronectin: position-specific activation of RGD/Synergy site-dependent migratory behavior at gastrulation. J. Cell Biol. *134*, 1–14.
30. Hoffstrom, B.G. (2002). Integrin function during *Xenopus laevis* gastrulation. PhD thesis, University of Virginia, Charlottesville, Virginia.
31. Schechtman, A.M. (1942). The mechanics of amphibian gastrulation I. Gastrulation-producing interactions between various regions of an anuran egg (*Ityla regila*). Univ. Calif. Pub. Zool. *51*, 1–39.
32. Keller, R.E. (1984). The cellular basis of gastrulation in *Xenopus laevis*: active, postinvolution convergence and extension by mediolateral interdigitation. Am. Zool. *24*, 589–603.
33. Davidson, L.A., Keller, R., and DeSimone, D. (2004). Patterning and tissue movements in a novel explant preparation of the marginal zone of *Xenopus laevis*. Gene Expr. Patterns *4*, 457–466.
34. Moriyoshi, K., Richards, L.J., Akazawa, C., O'Leary, D.D., and Nakanishi, S. (1996). Labeling neural cells using adenoviral gene transfer of membrane-targeted GFP. Neuron *16*, 255–260.
35. Bazzoni, G., Ma, L., Blue, M.L., and Hemler, M.E. (1998). Divalent cations and ligands induce conformational changes that are highly divergent among β_1 integrins. J. Biol. Chem. *273*, 6670–6678.
36. Gailit, J., and Ruoslahti, E. (1988). Regulation of the fibronectin receptor affinity by divalent cations. J. Biol. Chem. *263*, 12927–12932.
37. Sechler, J.L., Corbett, S.A., and Schwarzbauer, J.E. (1997). Modulatory roles for integrin activation and the synergy site of fibronectin during matrix assembly. Mol. Biol. Cell *8*, 2563–2573.
38. Moore, S.W., Keller, R.E., and Koehl, M.A.R. (1995). The dorsal involuting marginal zone stiffens anisotropically during its convergent extension in the gastrula of *Xenopus leavis*. Development *121*, 3130–3140.
39. Wacker, S., Grimm, K., Joos, T., and Winklbauer, R. (2000). Development and control of tissue separation at gastrulation in *Xenopus*. Dev. Biol. *224*, 428–439.
40. Zhong, Y., Brieher, W.M., and Gumbiner, B.M. (1999). Analysis of C-cadherin regulation during tissue morphogenesis with an activating antibody. J. Cell Biol. *144*, 351–359.
41. Mould, A.P., Akiyama, S.K., and Humphries, M.J. (1995). Regulation of integrin $\alpha_5\beta_1$-fibronectin interactions by divalent cations. Evidence for distinct classes of binding sites for Mn^{2+}, Mg^{2+}, and Ca^{2+}. J. Biol. Chem. *270*, 26270–26277.
42. Kay, B.K., and Peng, H.B. (1991). *Xenopus laevis*: Practical Uses in Cell and Molecular Biology, *Volume 36* (New York: Academic Press).
43. Nieuwkoop, P.D., and Faber, J. (1967). Normal Tables of *Xenopus laevis* (Daudin) (Amsterdam: Elsevier North-Holland Biomedical Press).
44. Wallingford, J.B., Rowning, B.A., Vogeli, K.M., Rothbacher, U., Fraser, S.E., and Harland, R.M. (2000). Dishevelled controls cell polarity during *Xenopus* gastrulation. Nature *405*, 81–85.
45. Sater, A.K., Steinhardt, R.A., and Keller, R. (1993). Induction of neuronal differentiation by planar signals in *Xenopus* embryos. Dev. Dyn. *197*, 268–280.
46. H.L. Sive, R.M. Grainger, and R.M. Harland, eds. (2000). Early Development of *Xenopus laevis*: A Laboratory Manual (Cold Spring Harbor, NY: Cold Spring Harbor Laboratory Press).
47. Laemmli, U.K. (1970). Cleavage of structural proteins during the assembly of the head of bacteriophage T4. Nature *227*, 680–685.
48. Hens, M.D., and DeSimone, D.W. (1995). Molecular analysis and developmental expression of the focal adhesion kinase pp125FAK in *Xenopus laevis*. Dev. Biol. *170*, 274–288.
49. Marcantonio, E.E., and Hynes, R.O. (1988). Antibodies to the conserved cytoplasmic domain of the integrin β_1 subunit react with proteins in vertebrates, invertebrates, and fungi. J. Cell Biol. *106*, 1765–1772.
50. Shih, J., and Keller, R. (1992). Patterns of cell motility in the organizer and dorsal mesoderm of *Xenopus laevis*. Development *116*, 915–930.
51. Ezin, A.M., Skoglund, P., and Keller, R. (2003). The midline (notochord and notoplate) patterns the cell motility underlying convergence and extension of the *Xenopus* neural plate. Dev. Biol. *256*, 100–114.
52. Zar, J.H. (1998). Biostatistical Analysis, 4th Edition (Upper Saddle River, NJ: Prentice-Hall).
53. Davidson, L.A., and Keller, R.E. (1999). Neural tube closure in *Xenopus laevis* involves medial migration, directed protrusive activity, cell intercalation and convergent extension. Development *126*, 4547–4556.
54. Russ, J.C. (1999). The Image Processing Handbook, 3rd Edition (Boca Raton, FL: CRC Press LLC).